JOURNAL OF GEOPHYSICAL RESEARCH, VOL. 87, NO. B5, PAGES 3663-3678, MAY 10, 1982

LITHOSPHERIC DEFORMATION WITHIN THE MOLUCCA SEA ARC-ARC COLLISION: EVIDENCE FROM SHALLOW AND INTERMEDIATE EARTHQUAKE ACTIVITY

Robert McCaffrey [1]

Earth Sciences Board, University of California, Santa Cruz, California 95064

Abstract. This paper presents the results of a local earthquake survey in the Molucca Sea arc-arc collision zone of eastern Indonesia. Although intermediate depth earthquakes define zones dipping to the west beneath the Sangihe arc and to the east beneath the Halmahera volcanic arc, only shallow activity (less than 60 km depth) occurred beneath the central part of the collision zone where the majority of activity is observed. The concentration of earthquake foci in the 10- to 50-km depth range in a limited region beneath the Talaud-Mayu Ridge suggests that convergence between the arcs proceeds by shortening within basement of the intervening Molucca Sea plate rather than by slip along shallow dipping planes between the arcs and the subducted slabs. Published focal mechanism solutions suggest that high-angle reverse faulting beneath the Talaud-Mayu Ridge generates almost all of the seismic energy release within the collision zone. The predominance of shallow reverse and strike slip faulting at the axis of the bilaterally subducting Molucca Sea lithosphere suggests that stresses are not due to bending alone and have a large horizontal regional component perpendicular to the island arcs. The geometry and state of stress within the Molucca Sea lithosphere requires an external driving force for the convergence between the two arcs and a strong degree of coupling between the island arcs and the subducting Molucca Sea plate, at least at the present stage of collision.

Introduction

The precise estimation of depths of earthquakes associated with collision zones is an important consideration in unraveling the mechanism of collision and implications for structure within present mountain belts. The inferred presence of intermediate depth earthquakes beneath the Zagros led Bird et al. [1975] to interpret deformation in that continent-continent collision as occurring in a fashion analogous to subduction of oceanic lithosphere with a subducting slab attached to the leading edge of the Arabian plate. Recent local earthquake surveys in the Zagros, however, have not found any activity deeper than 30 km [Von Dollen et al., 1977; Savage et al., 1977; Niazi et al., 1978], and modeling of teleseismic long-period body waves suggests the larger earthquakes are in the 8- to 15-km depth range [Jackson and Fitch, 1981], although intermediate depth earthquakes appear in routine locations of the International Seismological Centre for the same regions. The apparent presence of intermediate earthquakes is probably due to poor depth resolution of the World Wide Standard Seismograph Network for shallow earthquakes in the Zagros [Jackson and Fitch, 1979; Jackson, 1980].

Similarly, in the Molucca Sea arc-arc collision zone of eastern Indonesia (Figure 1), depths of earthquakes within the central, most active part of the collision zone are masked by the poor resolution inherent in the lack of nearby seismograph stations. This paper examines the depths of earthquakes beneath the Molucca Sea based on data from a temporary seismograph network operated within the collision zone. Also, a model for the active tectonics of the arc-arc collision is presented.

Structure and Tectonic Setting

Eastern Indonesia is situated in a zone of convergence between four major lithospheric plates, the Indian Ocean-Australian, Asian, Philippine Sea and Pacific plates. As a consequence, eastern Indonesia represents a wide region of deformation and includes many smaller plates and various presently active and completed collision events [Hamilton, 1979]. The collision between the Sangihe and Halmahera island arcs to the west and east sides of the Molucca Sea is presently under way and nearing completion (Figure 1).

Hamilton [1977, 1979] suggested that the Molucca Sea is underlain by severely deformed rocks as indicated by their irresolvable nature in reflection profiles, and reflection profiling by Silver and Moore [1978] clearly shows the symmetry of the collision zone. Silver and Moore [1978] suggest that the deformed material (collision complex) is spreading gravitationally away from the central bathymetric high, the Talaud-Mayu Ridge, toward the 3-km-deep trenches wherein thrust surfaces between the collision complex and the relatively undeformed island arc aprons crop out (Figure 2).

The internal structure of the collision zone, inferred from interpretations of seismic refraction and gravity profiles, is dominated by a very thick unit of low density, low seismic velocity material underlying the Molucca Sea [McCaffrey et al., 1980a]. The collision complex is 10-14 km thick in the central region of the Molucca Sea beneath the Talaud-Mayu Ridge and thins toward the island arcs. The complexity of travel time curves and severity of attenuation have been cited as further evidence for the highly sheared nature of the collision complex.

The Sangihe volcanic arc consists of active volcanoes from the north tip of the North Arm of Sulawesi to Sangihe (Figure 1). An inactive extension of the arc continues northward into

[1] Now at Department of Earth and Planetary Sciences, Massachusetts Institute of Technology, Cambridge, Massachusetts 02139

Paper number 1B1425.
0148-0227/82/001B-1425$05.00

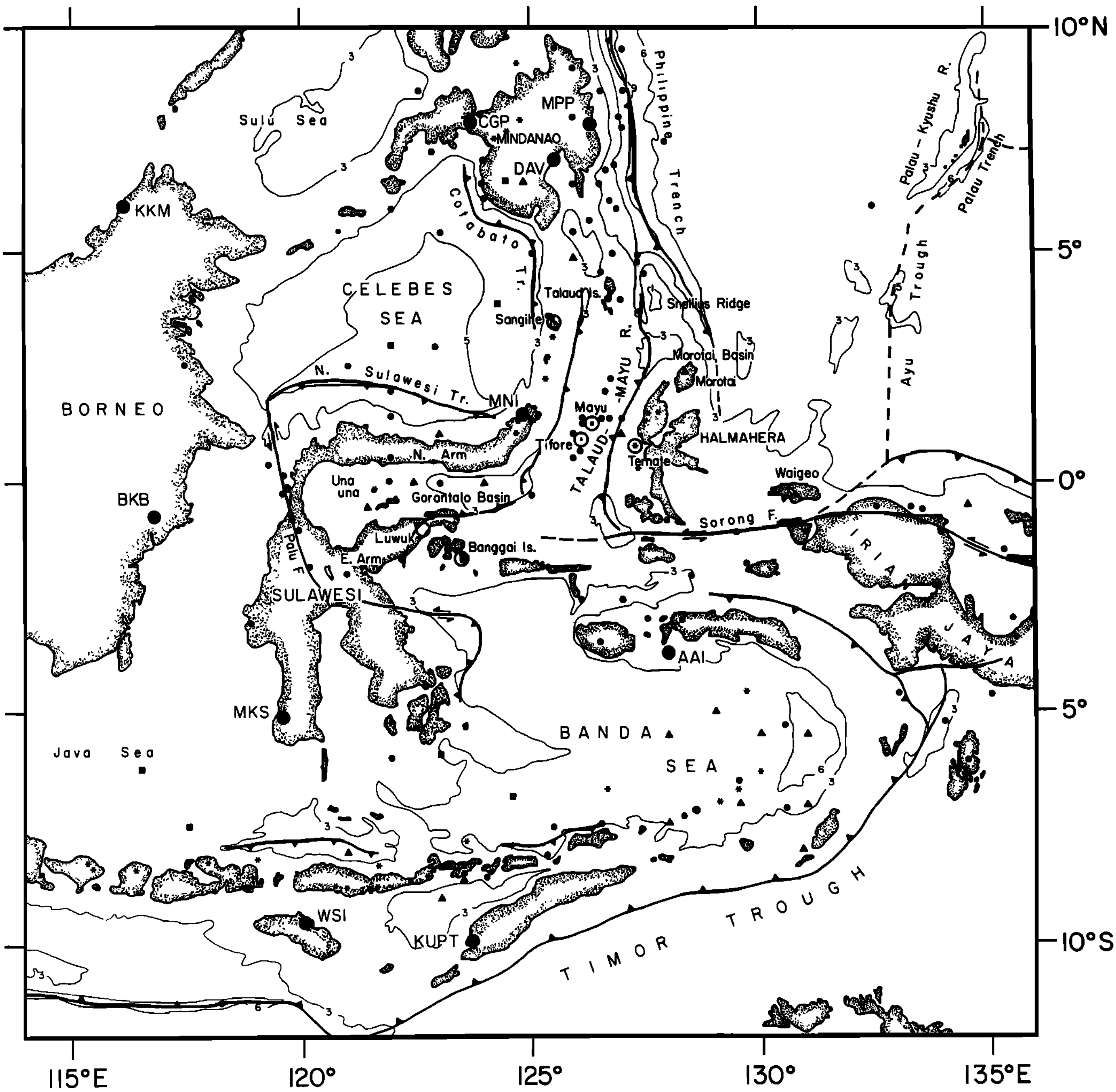

Fig. 1. Geographic and generalized tectonic map of eastern Indonesia. Thrust faults are shown with teeth on overriding plates and have been adapted from Hamilton [1979] and Silver [1981]. Active volcanoes are marked by asterisks. Solid small circles, triangles, and squares show locations of shallow, intermediate, and deep earthquakes, respectively, of magnitude greater than or equal to 7.0 for 1897-1977 from Duda [1965] and Bath and Duda [1979]. Bathymetric contours are as marked in kilometers taken from Hamilton [1979]. Large open and solid circles show positions of temporary and permanent seismograph stations, respectively.

Mindanao, where activity is again observed. Geochemical studies of the Sangihe arc reveal typical island arc type volcanism, suggesting that the collision so far has apparently had no unique effect on the geochemistry of the arc magmatism [Morrice and Gill, 1980]. The Halmahera volcanoes are active from 0.5°N to 1.7°N, but Quaternary centers extend southward to the Sorong Fault. Comparatively little is known of the composition of these volcanoes.

Seismicity of the Molucca Sea

The seismicity of northeastern Indonesia displays a wide variety of tectonic settings with abundant shallow, intermediate, and deep activity. The distribution of intermediate and deep earthquakes in eastern Indonesia has been previously reported by Hatherton and Dickinson [1969], Fitch [1970,1972], Fitch and Molnar [1970], Hamilton [1974], and an exhaustive study

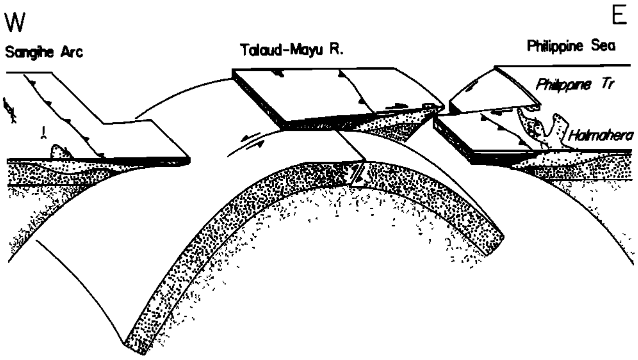

Fig. 2. Exploded block diagram of structure and tectonics of the Molucca Sea collision zone. The view is from the southwest and shows the Sangihe arc, Philippine Sea plate, and collision complex pulled away from the Molucca Sea lithosphere. The wavy line pattern represents collision complex, small-v pattern is island arc crust, heavy stippling is the mantle portion of the lithosphere, and light stippling represents asthenospheric material. All faults are indicated by arrows showing the sense of motion. Other breaks in the diagram are for purposes of exposition and do not represent structure. The northern and southern limits of this diagram are shown in Figure 10.

by Cardwell et al. [1980]. Figure 3 is a map and set of stereo plots of earthquake hypocenters for the Molucca Sea and vicinity taken from Bulletins of the International Seismological Centre (ISC) for the years 1964-1975 having more than 40 stations reporting. The intensity and widespread occurrence of seismic activity in the eastern Indonesian region reflects the rapid convergence (about 90 mm/year) between the Philippine Sea and Eurasian plates [Seno, 1977].

Intermediate and deep earthquakes define an inclined seismic zone dipping to the west beneath the Sangihe arc, and an intermediate zone dips to the east beneath northern Halmahera. The projections of these two seismic zones toward the surface intersect beneath the Talaud-Mayu Ridge in the central Molucca Sea. The reader is referred to the works of Hamilton [1974] and Cardwell et al. [1980] for more details on the distribution of deep activity in the region.

The Philippine Trench represents the major northeastern tectonic boundary of eastern Indonesia (Figure 1). Water depths in the trench exceed 9000 m east of Mindanao but shoal to the south to less than 6000 m behind Morotai and to 3000 m just east of the Northeast Arm of Halmahera. North of 3^{o}N, seismic activity is dense and indicates westward directed underthrusting of the Philippine Sea plate beneath the Philippine Islands and Snellius Ridge (Figure 3). The steep dip of earthquake foci along with the lack of significant activity at depths greater than 100 km, the absence of active volcanism [Cardwell et al., 1980], and the presence of a lobe of young turbidites east of the Philippine Trench [Karig, 1975] have been cited as evidence for the youthfulness of this tectonic feature.

To the west of the Sangihe arc and north of the island of Sangihe the morphological features of incipient subduction have been reported [Hamilton, 1979; Silver and Moore, 1978]. Furthermore, a major, shallow earthquake displaying a thrust type mechanism occurred along the Cotabato Trench (Figure 1) and has been interpreted as additional evidence for subduction behind the Sangihe arc west of Mindanao [Stewart and Cohn, 1979]. The completion of the collision process in the northwest is thus being told by the formation of a new convergent margin exterior to the collision zone.

Thrusting behind the Sangihe arc does not continue south of Sangihe (E. A. Silver, personal communication, 1978). In a similar fashion the Philippine Trench shallows to the south, and seismicity dies out at about 2.5^{o}N. In contrast to the broad scatter of earthquake foci around the Talaud Islands, seismicity in the central Molucca Sea, south of the latitude of Morotai, is quite dense and aligned along the Talaud-Mayu Ridge (Figure 3). In the region south of 2.6^{o}N, very little shallow activity can be associated with the areas adjacent to or behind the island arcs.

Although the line of active volcanoes on Halmahera defines an island arc type volcanic front from 0.3^{o}N to 1.5^{o}N and late Quaternary volcanoes extend further south, intermediate seismic activity is confined to the region beneath the North Arm and Northeast Arm of Halmahera, north of 1^{o}N and beneath the Snellius

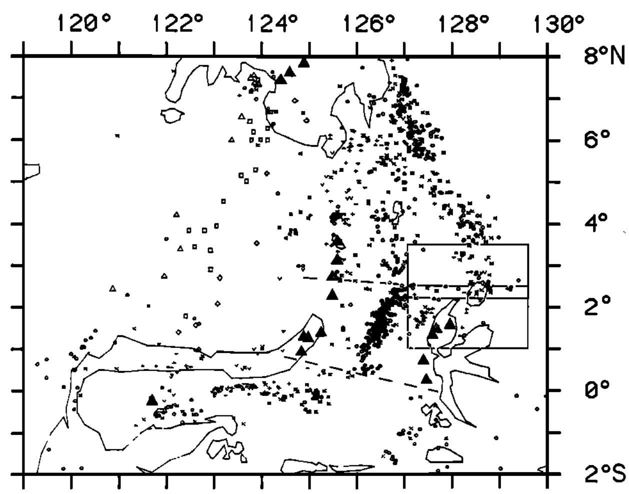

Fig. 3a. Map of earthquake epicenters taken from ISC Bulletins for the years 1964-1975 [International Seismological Centre, 1964-1975]. Each event shown was recorded by 40 or more stations of the World-Wide Standard Seismograph Network. Solid triangles show active volcanoes. Symbols representing depths are as follows: o = 0-60 km; x = 61-100 km; + = 101-200 km; v = 201-300 km; * = 301-400 km; diamond = 401-500 km; square = 501-600 km; small triangle = greater than 600 km. The box at the eastern edge of the Molucca Sea shows the area referred to in Figure 8. The dashed lines approximately perpendicular to the volcanic arcs divide the region into sectors which are referred to as the northern and central Molucca Sea and Gorontalo Basin, from north to south.

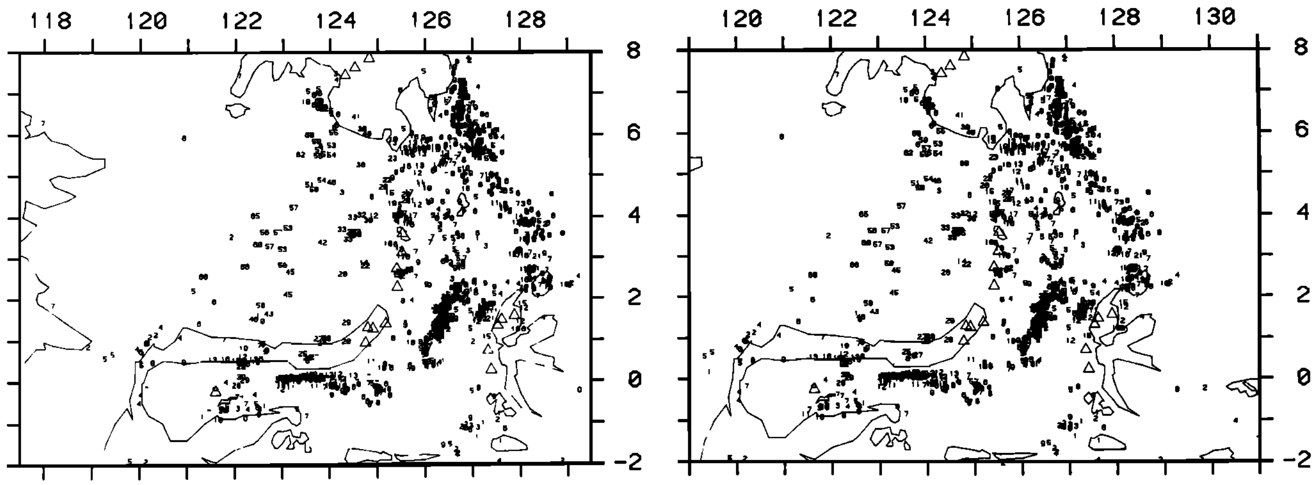

Fig. 3b. Stereo pair of the same data set plotted in Figure 3a. The symbols used to represent the events are the depths in tens of kilometers. Open triangles are active volcanoes.

Ridge north of Morotai (Figure 3) where there are no volcanoes. Later, evidence will be presented which suggests the presence of two separate east dipping slabs beneath the region of northern Halmahera and the Snellius Ridge.

In the southern Molucca Sea the zone of seismic activity decreases in intensity for a 70-km stretch and then turns toward the west and bisects the Gorontalo Basin (Figure 3) in an east-west zone along the equator from 122.8°E to 125.3°E. The most intense earthquake activity defines a nearly vertical zone which plunges to the west but not parallel to the direction of maximum dip of the seismic zone as observed in the north. These earthquakes, which are examined in a later section, probably outline the southern edge of the Molucca Sea plate subducted beneath the Sangihe island arc and suggest a clockwise (as viewed from above) contortion within the subducted slab possibly related to the collision zone (see Figure 3b). For discussions of earthquake activity in the western Gorontalo Basin, the reader is again referred to the works of Hamilton [1974,1979] and Cardwell et al. [1980].

The Local Earthquake Survey

Data Analysis

A 3-week local earthquake survey was conducted in the Molucca Sea of eastern Indonesia during November and December of 1978 [McCaffrey et al., 1980b]. Detailed descriptions of the field study and data analysis are given in the appendix and are only summarized here. The main purpose of the study was to determine the depth of seismicity beneath the Talaud-Mayu Ridge, and to this end stations were operated on the small islands of Mayu and Tifore (Figure 1) directly above the area of most intense earthquake activity. The locations of permanent and temporary stations are shown in Figure 1.

Tests were run on both real and synthesized data in order to estimate the limits on accuracy which can be expected and also to filter out poorly constrained locations. First, a local velocity model was constructed based on refraction studies in the Molucca Sea [McCaffrey et al., 1980a] and used to calculate travel times to the stations at Mayu and Tifore because of their positions within the structurally complex collision zone and their importance in the determination of depths. All other travel times were based on the tables of Herrin et al. [1968] for P and Jeffreys and Bullen [1958] for S. Fifteen of the most widely recorded events were located by the method of joint hypocenter determination (JHD) [Dewey, 1971] in the hopes of removing systematic errors in the travel time curves by generating station corrections. Using the station delays generated by the JHD run, all earthquakes were located by a single-event least squares location scheme [Bolt, 1960] 20 times while adding normally distributed random errors with a variance of 1.0 s to all arrival times. Means and standard deviations for latitude, longitude, depth, and origin time and standard error were calculated for each event. Events with a standard deviation of greater than 40 km in latitude, longitude, or depth are considered unreliable and are not presented. Plots of recorded events with error bars corresponding to one standard deviation in length are shown in Figures 4b, 5b, and 6b.

A parallel analysis was performed on 18 events generated at six epicentral locations (Figure A1) and three depths (10, 50, and 100 km). In order to estimate the effect of using an inaccurate velocity model, the velocity model used to generate the arrival times of the test events was much 'faster' than the model used in locating them (Table A1), and this introduced a shallowing effect on all hypocenters (except those at 10-km depth) which even station corrections generated by the JHD could not remove (Figure A2). One very significant result of this analysis is that only in the region close to Mayu and Tifore (for instance, position 2 in Figure A1) can the array distinguish between events at 10- and 50-km depth, but it is still quite insensitive to the depths of the shallowest events. The systematic miscalculation of depth (around 10 km) for the test events at 50- and 100-km depth is probably

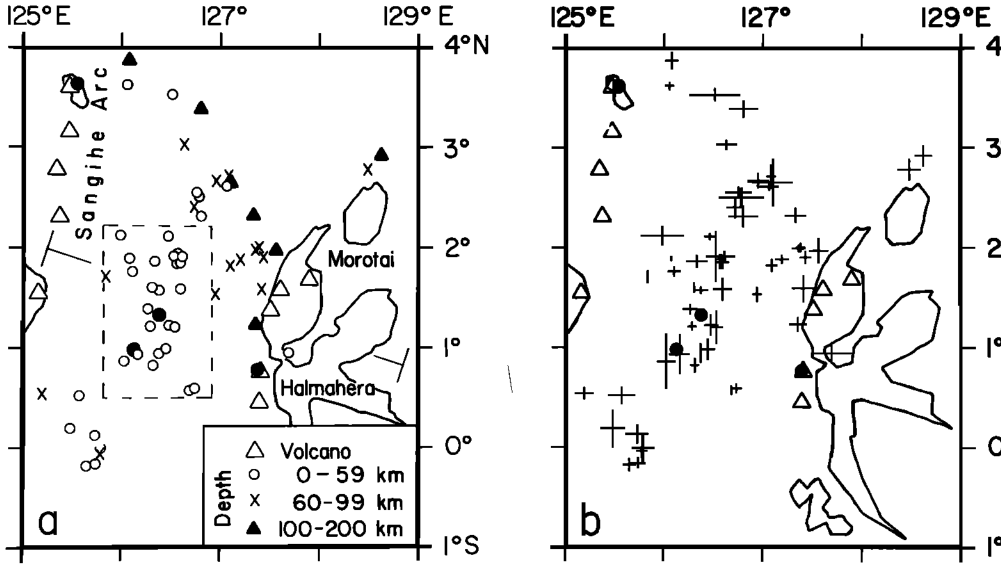

Fig. 4. (a) Map of earthquake epicenters recorded during the local earthquake survey. The locations of temporary stations are shown by solid circles. The small box in the central Molucca Sea shows the area covered in Figure 6. The brackets on either side of the figure show the projection angle in Figures 5 and 6. (b) Error bars of one standard deviation for each event.

close to the maximum to be expected for the real data because the pronounced difference in the two velocity models (Table A1) used to generate and locate these events is likely greater than the uncertainty in the estimate of the true velocity model.

Results

Earthquake activity associated with the Molucca Sea collision zone is confined to the upper 60 km of lithosphere beneath the Talaud-Mayu Ridge and to zones dipping beneath the Sangihe and Halmahera island arcs. Intermediate activity is confined mainly to the region north of 1°N on the Halmahera side of the collision zone (Figure 4). As shown in Figure 5, a vertical projection perpendicular to the island arcs, seismic zones dip west beneath the Sangihe arc and east beneath Halmahera. Hypocenters from the local survey in the Molucca Sea show a rather broad zone extending to at least 100-km depth

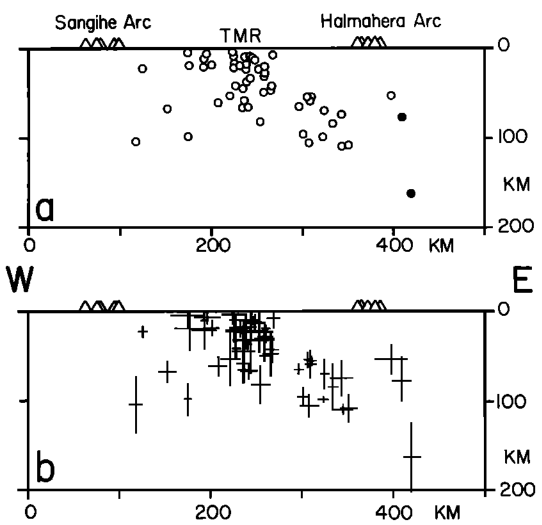

Fig. 5. (a) Projection of all earthquakes shown in Figure 4 onto a vertical plane striking N70°W, perpendicular to the island arcs and the Talaud-Mayu Ridge (TMR). Active volcanoes are shown by triangles at the surface. The two events shown as solid circles occurred north of Morotai. (b) Error bars of one standard deviation for each event.

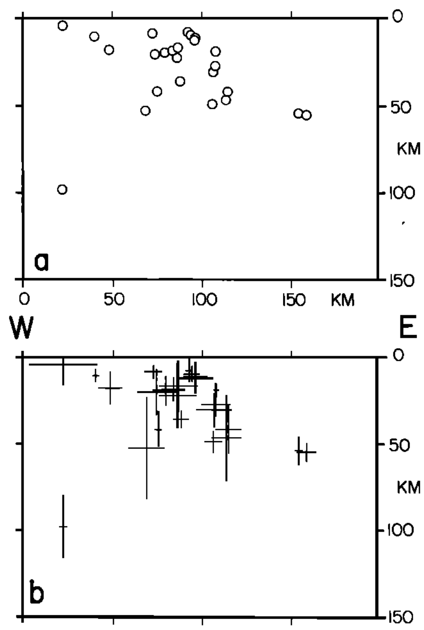

Fig. 6. (a) Projection of earthquakes beneath the Talaud-Mayu Ridge from 0.5°N to 2.2°N and 125.8°E to 126.9°E (see small box in Figure 4a) onto a vertical plane perpendicular to the island arcs. (b) Error bars of one standard deviation for each event.

beneath Halmahera, but all foci occur between 1.0°N and 2.2°N (Figure 4). Interestingly, no earthquakes were recorded from beneath the volcanoes on Halmahera. All intermediate events occurred seaward of the volcanic front except two earthquakes which are located at 75- and 163-km depth north of Morotai (shown as solid circles in Figure 5a).

Very little activity was recorded from beneath the Sangihe arc (Figure 5). Some of the shallow events which project to the area just east of the Sangihe arc are from the Talaud Islands-Sangihe region. Differences between S and P arrival times indicate little activity near the island arcs during the survey, as intervals less than 10 s (approximately 80 km) were absent from the stations on Sangihe and Ternate and none less than 14 s were recorded at station MNI. S-P times as short as 1 s were observed at the stations at Mayu and Tifore.

The most pronounced activity observed in the Molucca Sea is clearly at the apex of the inverted-V-shaped seismic zone at shallow depths beneath the Talaud-Mayu Ridge. Figure 4 shows that most of this activity lies along the Talaud-Mayu Ridge between 0.5°N and 2.0°N.

Depth of Seismicity Beneath the Talaud-Mayu Ridge

Figure 6 shows a vertical section of seismicity beneath the central Molucca Sea from 0.5°N to 2.2°N and 125.8°E to 126.9°E projected onto a plane striking N70°W, perpendicular to the Talaud-Mayu Ridge. The importance of this region lies in that it is the most seismically active

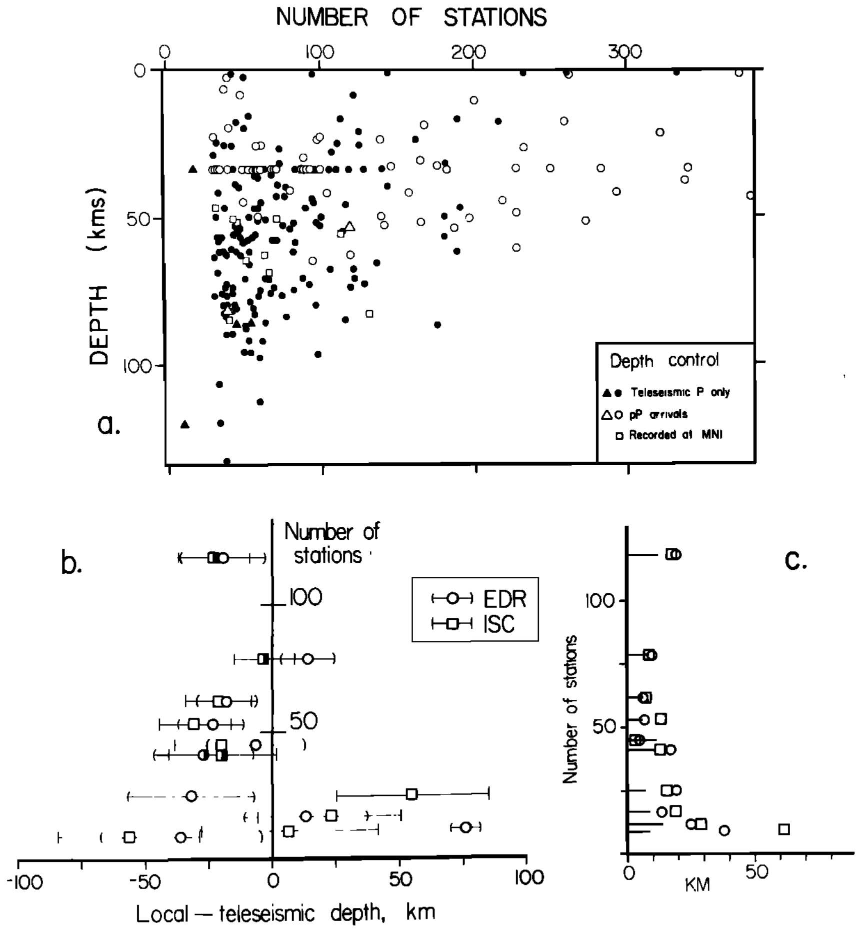

Fig. 7. (a) Plot of ISC depth versus number of stations used to locate the event for earthquakes occurring beneath the Talaud-Mayu Ridge from 1964 to 1975. The minimum number of stations considered is 30 hence the absence of data below this value. Different symbols are used to distinguish the types of depth control as shown in the legend, and triangles are ISC depths of earthquakes which occurred during the local survey period. In the region represented by this plot, no earthquakes deeper than 60 km were recorded during the local survey. (b) Differences between ISC and EDR computed depths for Molucca Sea earthquakes and those from the local survey. Error bars are the sums of errors in depth computed for the local network locations plus those given in the ISC Bulletin or EDR. (c) Differences in kilometers between epicentral position of ISC and EDR locations compared to local network determinations. Horizontal lines extending from the ordinate axis are the epicentral errors for the locations with local data. Relative positions for some of these events can be seen in Figure A3.

Table 1. Depths Determined by the Local Survey Compared with those Taken from ISC Bulletins and the EDR

		Local						EDR		ISC			
		Latitude, deg		Longitude, deg		Depth, km		Depth, km		Depth, km			
Date, 1978	Time	M	SD	M	SD	M	SD	M	SD	M	SD	M_b	N
Nov. 21	0357	3.03	0.05	126.63	0.10	60	11	87*	9	80*	10	5.1	41
Nov. 21	0442	1.97	0.12	127.56	0.09	109	6	33		102	29	5.1	12
Nov. 21	1259	-0.04	0.07	125.78	0.05	65	13	52	11	41	15	5.3	17
Nov. 21	1549	-0.18	0.06	125.65	0.06	18	15	50	10	73	15	5.3	25
Nov. 21	1728	-0.16	0.05	125.74	0.07	57	5	43	6	60*	7	5.0	78
Nov. 21	1840	1.53	0.07	126.94	0.04	64	6	100	26	120	22		9
Nov. 22	0007	1.58	0.11	126.59	0.09	30	10	50	7	54*	4	5.3	118
Nov. 22	1643	0.59	0.04	126.73	0.05	55	5	79	8	86	9	5.2	53
Dec. 01	1843	2.40	0.10	126.72	0.08	66	9	73	10	86	10	4.9	45
Dec. 07	1648	1.99	0.03	127.36	0.06	98	4	116	8	119	9	5.1	62

N is the number of stations recording the event. M is the mean, and SD is the standard deviation.
* pP data used.

area in the Molucca Sea (Figures 3 and 4) and it is the area within which the seismograph array displays the most depth sensitivity. The maximum mean depth for any event in this region is around 50 km except for one event at 100 km which occurs within the slab dipping beneath the Sangihe arc. Tests with synthetic data have shown that errors in the velocity model may produce systematic errors as large as 10 km in depth for events at 50-km depth and, taking this into consideration, suggests that the maximum depth of seismicity beneath the Talaud-Mayu Ridge is no greater than 60 km but could be as shallow as 40 km. ISC locations (Figure 3) give depths in excess of 100 km in the same region. I suggest that intermediate depth events reported in the ISC Bulletins are probably mislocated and that the maximum depth required by existing data is 60 km. This contention is not surprising, since the closest station available for use in ISC locations (MNI at Manado (Figure 1)) is over 150 km distant and has been in operation only since 1974. Even at this distance the depth sensitivity of the MNI station is negligible for events at 60-km depth. As shown in Figure 7a, a plot of depth against the number of recording stations for ISC locations, the deepest event reported in ISC Bulletins within the same region as Figure 6 that was recorded at station MNI is at 80-km depth. At this depth, however, the MNI station has a sensitivity to depth of ±30 km if the calculated travel time to the station is different from the true travel time by 1 s or more, which implies that this event could have occurred at 50-km depth or less.

In the absence of nearby stations, reliable depth phases such as pP or sP must be used to determine depth. In Figure 7a the envelope of the maximum depth of events decreases with an increasing number of stations and with the presence of pP phases. The maximum depth of an event recorded by greater than 200 stations or with pP arrivals is 70 km, and this depth could be tens of kilometers shallower owing to the uncertainties in crustal structure below the Talaud-Mayu Ridge. Since the number of stations recording an earthquake may be crudely related to its size, it might be argued that only small earthquakes occur at depths greater than 70 km. Considering that no earthquakes deeper than 60 km were located beneath the Talaud-Mayu Ridge during the local survey, I suggest that the appearance of intermediate events in ISC Bulletins for this region is merely an artifact of the earthquake location procedure resulting from poor depth control.

Table 1 and Figure 7b compare depths computed by the local survey with those taken from the ISC Bulletins and the Earthquake Data Report (EDR) of the U.S. Geological Survey [1978] for the same events. For events recorded by less than 30 stations, errors in focal depths seem to be large and randomly distributed. When greater than 30 or 40 stations record the event, there is a slight preference for the mean EDR and ISC depth calculations to be greater than the locally determined mean depth by 20-30 km. The error bars on each event in Figure 7b represent the sum of the errors for the locally determined hypocenter plus the EDR or ISC reported errors. There may also be a systematic error of 10 km in the depth of the locally determined hypocenters, in which case almost all the error bars in Figure 7b for events recorded by greater than 40 stations intersect zero.

Figure 7c shows the differences between epicentral positions of the ISC and EDR locations and the locally determined epicenters plotted against the number of stations recording the event. Again, only for events located by less than 40 stations do the differences in epicentral position become significant (with respect to errors in locating the events with local travel time data).

Implications for the Active Tectonics of the Arc-Arc Collision

The results of the local earthquake survey in the Molucca Sea provide some valuable insight into the mechanics of arc-arc collision. The most important results are the constraints on the depth at which seismicity occurs beneath the central Talaud-Mayu Ridge (less than 60 km) and the spatial distribution of earthquakes within the collision zone. Using this information along with longer term seismicity patterns from ISC Bulletins (Figure 3), I suggest that the collision between the Sangihe and Halmahera arcs occurs as described in the following paragraphs.

Northern Molucca Sea

From Morotai to about 3.5°N a steep east dipping seismic zone is present beneath the Snellius Ridge, but this zone is separate from the zone beneath Halmahera. Figure 8 shows projections of ISC earthquakes (Figure 3) in the region from 1.0°N to 3.5°N and east of 127°E separated into three groups: a northern group, north of 2.5°N (open circles in Figure 8), a transition group (half-solid circles), and a southern group, south of 2.2°N (solid circles). Figure 8a is projected at N70°W, perpendicular to the Sangihe and Halmahera island arcs. This projection shows earthquakes scattered possibly within a single east dipping zone. In an east-west projection (Figure 8b), however, the earthquakes appear to define two distinct east dipping zones: one in the south beneath Halmahera and a more steeply dipping zone to the north which underlies the shallow seismicity associated with the Philippine Trench. Seven earthquakes from the southern group occur at shallow and intermediate depths beneath southern Halmahera and appear to form a west dipping zone in Figure 8a. These events are well located [Cardwell et al., 1980], but their relationship to the tectonics of Halmahera is ambiguous.

One additional piece of evidence for a discontinuity in the slab subducted to the east of the Molucca Sea is the contrast in the propagation of shear waves to Ternate from an intermediate earthquake north of Morotai with those from northwest Halmahera. Intermediate events from northwest of Halmahera are characterized by efficient propagation of S to Ternate (Figure 8c), whereas the event from north of Morotai shows no S at all. The seismograph station at Ternate was not operating when the second intermediate event occurred north of Morotai. Seismograms for earthquakes north of Morotai recorded at Mayu also show high attenuation of S, whereas S was well developed from events beneath northwest Halmahera. Shear waves from the event north of Morotai shown in Figure 8c, however, were quite conspicuous on the record at Sangihe. The marked contrast in shear wave propagation from the two regions suggests that the energy traverses material with quite different elastic properties and may indicate that energy from earthquakes north of Morotai must propagate partially through the asthenosphere rather than completely within a cold lithospheric slab en route to Ternate and Mayu. I interpret this northern seismic zone as evidence for a remnant subducted slab beneath the Snellius Ridge.

Earthquake foci from the intermediate zone north of Morotai merge with those of the Philippine Trench at shallow depths and project upward into the seismically quiet region of the Snellius Ridge east of the Talaud Islands (Figure 8b). The position of the remnant slab with respect to surface features suggests that it may have been subducted eastward beneath the Snellius Ridge and subduction ceased when the Snellius Ridge entered the collision zone. Convergence may have then become centered at the Philippine

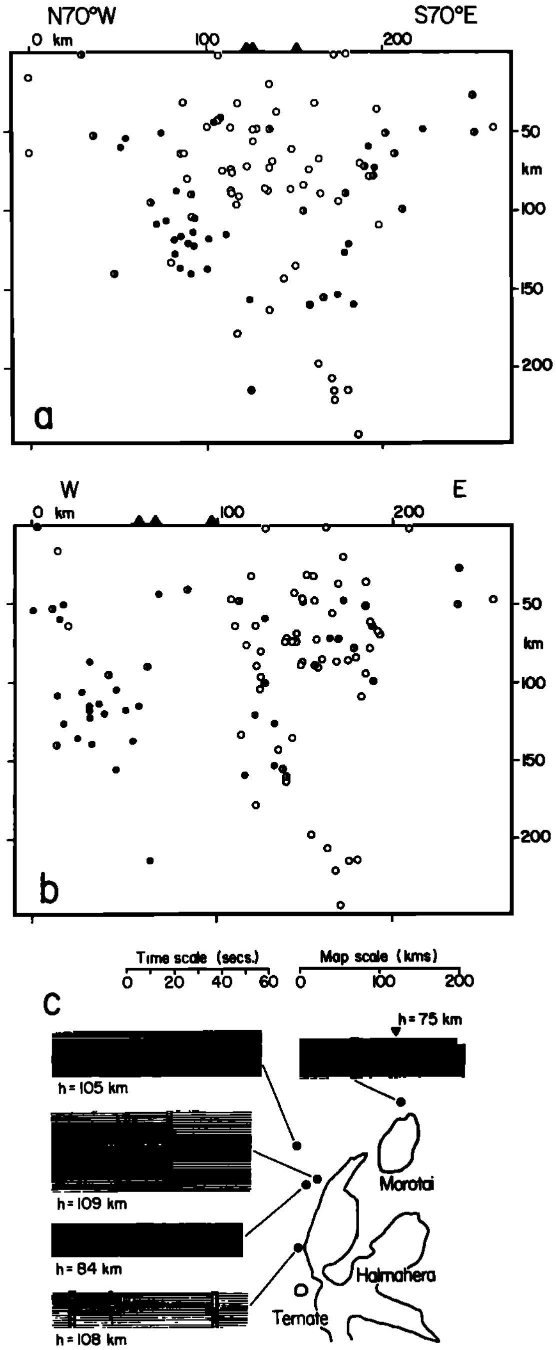

Fig. 8. Projections of ISC earthquakes occurring in the region from 1.0°N to 3.5°N and 127°E to 129.5°E. (a) Projection onto a plane striking N70°W. (b) Projection onto an east-west striking vertical plane. The area of concern is outlined in Figure 3a. Solid circles are events which occurred south of 2.2°N, half-solid circles are those which occurred between 2.2°N and 2.5°N, and open circles are those which occurred south of 2.2°N. All volcanoes shown at the surface are found south of 2.2°N on Halmahera. (c) Seismograms from intermediate earthquakes recorded at Ternate. Note the lack of S (expected arrival time shown by triangle) from the earthquake north of Morotai, whereas S is well developed in earthquakes from the region west of northern Halmahera.

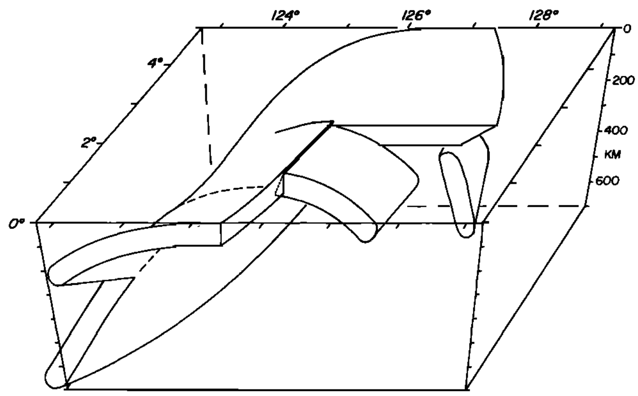

Fig. 9. Block diagram interpretation of the shape of the Molucca Sea lithosphere at the present time.

Trench east of the Snellius Ridge. Figure 9 shows a block diagram interpretation of the shape of the Molucca Sea lithosphere inferred from the distribution of earthquakes, and Figure 10 shows the preferred tectonic boundaries and contours of seismic zones for the collision zone.

The steep east dipping mantle seismic zone north of Morotai is observable to about 3.2°N. Thrusts between the collision complex and the two island arc aprons and the severe deformation of the surface rocks beneath the Molucca Sea are likewise not observed north of this latitude [Silver, 1981]. Thus a general connection may be involved between the limits of the presently active and recently completed arc-arc collision (as defined by oppositely dipping seismic zones) and the highly deformed collision complex at least at the northern boundary near the Talaud Islands. As expected, recent deformation within the collision zone is evident only where the island arcs are presently or have recently been converging south of the Talaud Islands. North of the Talaud Islands the majority of shortening is accommodated at the Philippine and Cotabato trenches exterior to the collision zone, and recent deformation is not apparent within the collision zone. The Philippine Trench east of the Snellius Ridge may have been activated following the cessation of convergence between the Molucca Sea plate and the Snellius Ridge and may in its present configuration be quite young.

A broad zone of shallow earthquakes is present beneath the Talaud-Mayu Ridge between the Talaud Islands and the Sangihe arc (Figure 3). These earthquakes form a west dipping zone and resemble other regions, such as the Aleutians [Engdahl, 1977], where active subduction is taking place. Thus the earthquakes between the Talaud Islands and Sangihe may represent continued subduction of the northern Molucca Sea plate beneath the Sangihe arc.

Central Molucca Sea

Seismicity associated with the Philippine Trench ceases south of about 2.5°N and the main form of seismic energy release shifts to high-angle reverse faulting beneath the central Molucca Sea. In addition, 2.5°N marks the northernmost limit of intermediate activity beneath Halmahera (Figures 3 and 4). Published focal plane solutions for earthquakes occurring beneath the central Talaud-Mayu Ridge are characterized by high-angle reverse mechanisms with horizontal B axes aligned roughly parallel to the north-northeast trend of the ridge (Figure 11) [Fitch, 1972; Cardwell et al., 1980]. On the Sangihe side of the central Talaud-Mayu Ridge, little shallow seismic activity is observed south of 2.5°N (Figures 3 and 4)[Cardwell et al., 1980, Figures 2 and 3], suggesting that convergence between the Molucca Sea plate and the Sangihe arc is aseismic, episodic, or not occurring. A magnitude 7.0 earthquake occurred west of the Talaud-Mayu Ridge (1.5°N, 125.5°E, h = 170 km) in August 1958, which may be related to subduction beneath the Sangihe arc just east of the North Arm but is probably too deep to be a thrust event. Similarly, a $M = 7.9$ earthquake is reported to have taken place just west of Ternate in 1907, although the depth is reported at 200 km by Duda [1965]. In the 80-year period from 1897 to 1977, 10 $M \geq 7.0$ earthquakes occurred along the Talaud-Mayu Ridge, including the $M = 8.3$ event of May 14, 1932 (Figure 1) [Duda, 1965; Bath and Duda, 1979]. The epicentral distributions of great earthquakes (Figure 1), ISC earthquakes (Figure 3), and locally recorded earthquakes (Figure 4) are quite similar within the collision zone.

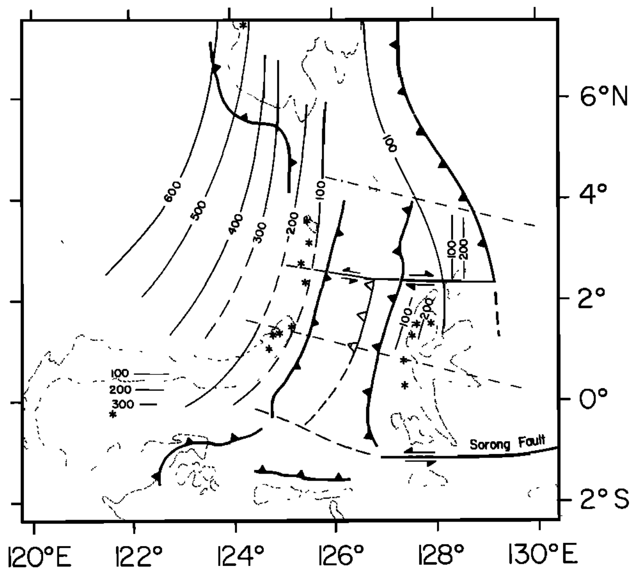

Fig. 10. Tectonic map of the Molucca Sea collision zone. Asterisks indicate active volcanoes. Surface boundaries are shown by heavy solid lines and solid teeth on the overriding plate of thrust boundaries. Lighter lines, small arrows, and open teeth refer to tectonic boundaries within the buried Molucca Sea plate. Lines are dashed where boundaries are inferred. Contours to the tops of seismic zones are labeled in kilometers and are modified from Cardwell et al. [1980]. Contours are dashed where interpolated or extrapolated because of insufficient data to resolve the seismic zone. The dash-dot lines through the central and northern Molucca Sea outline the southern and northern limits of the block diagram of Figure 2.

The conspicuous change in patterns of seismicity at 2.5°N (Figure 3) is coincident with marked changes in the free-air gravity field and bathymetry of the Molucca Sea. Relative highs in bathymetry [Mammerickx et al., 1976; E. A. Silver, unpublished data, 1981] and free-air gravity [Watts et al., 1978; McCaffrey et al., 1980a] are observed west of the zone of intense seismic activity beneath the Talaud-Mayu Ridge, whereas the rest of the Molucca Sea is characterized by low gravity and slightly deeper water. The boundaries of the highs coincide with the discontinuities in earthquake patterns (Figure 3). I suggest that basement underlying the western Molucca Sea between 1.0°N and 2.5°N is upraised relative to the rest of the Molucca Sea plate as shown in Figure 2.

Major convergence is being accommodated within the central Molucca Sea plate by high-angle reverse faulting beneath the Talaud-Mayu Ridge (Figure 11). Minor convergence may also occur between the eastern Molucca Sea slab and Halmahera (considered to be part of the Philippine Sea plate). The geometry suggested above requires a right-lateral transform fault to connect the Philippine Trench with either the reverse fault in the central Molucca Sea or the thrust between the Molucca Sea plate and Halmahera. Cardwell et al. [1980] suggest a transform connecting the Philippine Trench with the central Molucca Sea but picture it as lying farther to the north and connecting with the Ayu Trough (Figure 1) in the western Caroline Basin. I suggest that the transform proposed by Cardwell et al. [1980] passes through or close to Morotai at the southern edge of the Morotai Basin and stops at the Philippine Trench. Reasons for this re-interpretation are that shallow earthquakes are observed near Morotai, indicating that the Philippine Trench extends southward at least to the latitude of Morotai and a sparse yet linear zone of shallow earthquakes extends from the northern edge of the central Molucca Sea seismic zone into Morotai (Figure 3). This east-west trending zone of shallow earthquakes forms the

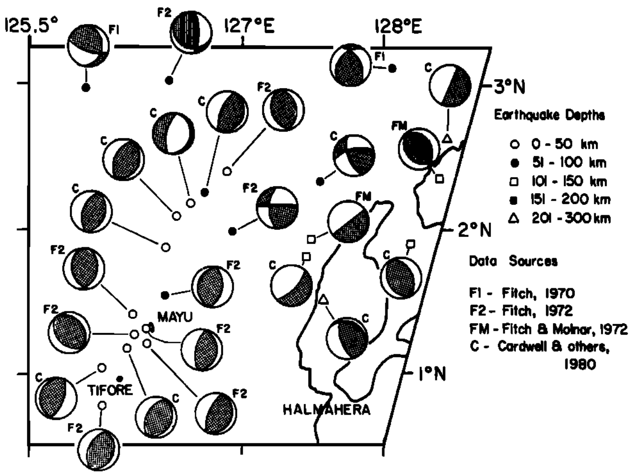

Fig. 11. Published focal mechanism solutions for earthquakes in the Molucca Sea. Depths given are from the original references cited. Shaded areas are compressional quadrants. Note the predominance of thrust faulting near Mayu and Tifore beneath the Talaud-Mayu Ridge.

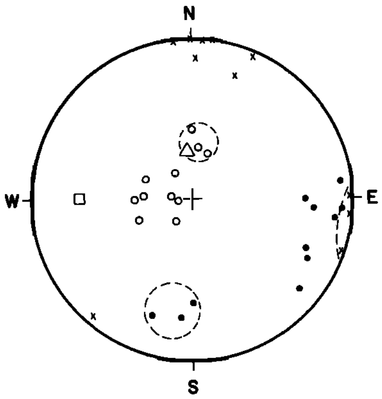

Fig. 12. Equal area projection on the lower focal hemisphere of P (solid circles), T (open circles), and B (crosses) axes from published focal plane solutions to earthquakes occurring in the Gorontalo Basin east of 123°E. The open square shows the orientation of the seismic zone in the east Gorontalo Basin, and the open triangle shows the orientation of the slab in the direction of maximum dip near the western end of the seismic zone. The three events whose principal axes directions are circled by dashed lines occur west of 123.8°E and deeper than 130 km. All other events shown occur east of 123.8°E and shallower than 102 km.

southern perimeter of a seismically quiet area between the Talaud-Mayu Ridge and the Philippine Trench. Also, there is no seismological evidence to suggest a transform extending east of the Philippine Trench.

If the Molucca Sea plate and the Sangihe arc are converging north of 2.5°N and coupled south of that latitude, then relative motion between basement of the northern and central Molucca Sea must be occurring (Figures 2 and 10). Focal mechanisms and changes in earthquake patterns suggest that a lateral tear or discontinuity may be present in the subducting slab beneath the Sangihe arc at about 2.5°N, allowing the northern part of the Molucca Sea plate to move to the west and down relative to the central Molucca Sea. The intermediate activity beneath the Celebes Basin changes character at about 2.5°N as the continuation of the seismic zone southward projects into a zone of conspicuous quiescence. Only two intermediate earthquakes are shown in Figure 3 beneath the Celebes Sea south of 3.0°N, whereas activity is well defined to the north. This quiescence west of the active arc-arc collision may mark some fundamental change in the character of the slab, but the details are a mystery. Kelleher and McCann [1976] have noted that, in general, gaps in intermediate depth seismic activity are present where bathymetric highs intersect trenches. The elevated basement west of the Talaud-Mayu Ridge may be acting as one such bathymetric high in that it is strongly coupled to the Sangihe arc. Two focal mechanism solutions published by Fitch [1970, 1972] (shown in the northwest corner of Figure 11) are consistent with a nearly east-west trending fault within the slab at about 3.0°N and suggest southward directed underthrusting with about 25% left-lateral motion. Also, seismic refraction profiles [McCaffrey et al., 1980a] and free-air gravity [Watts et al., 1978] are best interpreted by a substantial thickening of the collision complex to the north across the inferred fault zone.

The seismic zone beneath the Talaud-Mayu Ridge in the central Molucca Sea dies out to the south between 1.0°N and 0.5°N. The gravity field and bathymetry [Mammerickx et al., 1976; Watts et al., 1978; E. A. Silver, unpublished data, 1981] over the Molucca Sea drop off at this latitude, suggesting a deepening of basement south of 1.0°N. Furthermore, 1.0°N may mark the southern edge of the arc-arc collision because no earthquake activity is evident from beneath Halmahera south of this latitude (Figures 3 and 4). Active and Quaternary volcanoes, however, continue about 200 km southward to the Sorong Fault [Hamilton, 1979].

Gorontalo Basin

The seismically active zone jumps from the central Molucca Sea to the central Gorontalo Basin south of 1.0°N. The Gorontalo Basin is underlain by 2-3 km of low-velocity sediments [McCaffrey et al., 1981], the upper half of which are undeformed [Silver, 1981]. The southern edge of the Gorontalo Basin abuts the collision zone between the Banggai Islands and the East Arm of Sulawesi. Nearly all seismic activity in the eastern Gorontalo Basin occurs at intermediate depths and probably outlines the southern edge of the Molucca Sea plate subducted from the east beneath the North Arm. A sparse zone of intermediate depth earthquakes merges with the Gorontalo Basin seismic zone at about its maximum depth (about 300 km) and appears to connect with the slab beneath the Celebes Sea (Figure 3). The inferred geometry of the subducted Molucca Sea lithosphere is shown in Figure 9. I suggest that the earthquakes beneath the Gorontalo Basin represent a contorted tab of lithosphere attached to the Molucca Sea plate. The westerly plunge of the Gorontalo Basin seismic zone is much shallower than the dip of the subducted lithosphere to the north, suggesting that the slab is bent upward at its southern end. The inferred bend in the slab is best seen in the stereo pair plots of Figure 3b.

Maximum compressive stress (P) axes from published focal plane solutions (Figure 12) in the eastern Gorontalo Basin for earthquakes at depths of less than 100 km suggest east-west convergence and are nearly identical to those found in the central Molucca Sea [Cardwell et al., 1980], probably indicative of the regional stress field within the collision zone. West of 123.8°E and at depths in excess of 100 km, however, a dramatic change in the orientation of principal stress occurs within the seismic zone as the axes rotate clockwise nearly 90° about a vertical pole until the T axis becomes oriented downdip and the B axis along strike of the slab (Figure 12). The reorientation of stresses within the subducting lithosphere below 100-km depth is interpreted as the change from the east-west compressional regime of the surficial tectonics in this area to downdip extension within the sinking slab. The reorientation of the principal axes is additional evidence for the slab geometry shown in Figure 9. In Figure 9 the slab beneath the Gorontalo Basin is shown as being continuous with the deeper portions of the slab beneath the Celebes Sea, but the connection is ambiguous at present. The contortion of the southern end of the Molucca Sea plate beneath the North Arm and Gorontalo Basin is similar to bends in the northern end of the Tonga slab [Sykes et al., 1969] and southern New Hebrides arc [Pascal et al., 1978].

Mechanics of Arc-Arc Collision

The presently active arc-arc collision in the central Molucca Sea exhibits several features which are used to characterize the collision zone. Shortening across the collision zone appears to occur mainly by high-angle reverse faulting within the upper 40 km of the subducted Molucca Sea lithosphere at its apex. The lack of seismicity even at the microearthquake level suggests that convergence between the island arcs and the Molucca Sea plate along the usual low-angle, arcward dipping thrusts is either aseismic or is not occurring. Basement (most likely oceanic) beneath the western side of the Talaud-Mayu Ridge is apparently uplifted relative to the east, north, and south and may be strongly coupled to the Sangihe arc. Intermediate seismic activity beneath Halmahera is more pronounced than beneath the corresponding section of the Sangihe arc but is limited to the region between 1.0°N and 2.2°N. No focal plane solutions have been found to suggest active subduction of the Molucca Sea plate beneath the Halmahera or Sangihe arcs in the central part of the collision zone.

The foregoing features can be explained by a collision mechanism in which the shape of the bilaterally subducted lithosphere (Figure 2) of the Molucca Sea plate acts to inhibit asthenospheric counterflow away from the sinking lithosphere. The saddle shape of the slab may prevent it from sinking fast enough to accommodate the externally controlled rapid convergence between the island arcs. In such a case, horizontal stresses will be transmitted from the island arcs to the Molucca Sea lithosphere, resulting in horizontal compressive failure within the Molucca Sea plate as observed beneath the Talaud-Mayu Ridge. I suggest that the Molucca Sea plate may have become strongly coupled to the island arcs sometime following the onset of eastward subduction beneath Halmahera and that thrusting shifted to the central part of the plate as the increasingly tighter bend of the plate inhibited its vertical sinking.

A similar development may have occurred in the now completed portion of the arc-arc collision north of Morotai. The major difference, which may be a fundamental controlling factor in arc polarity reversal, is that convergence in the northern half of the collision zone near the Snellius Ridge was apparently taken up in the back arc at the Philippine Trench following collision. In the back arc region behind the Halmahera arc, opposite the collision zone, however, water depths are shallow, suggesting lighter crust which may not be as readily subductable as the oceanic lithosphere of the Philippine Sea plate to the north. In the

Halmahera case, continued convergence probably was taken up at the weakest point at the apex of the bilaterally subducting lithosphere in the central Molucca Sea. Thus the structure of the back arc region may have played a very important role in shaping the development of this collision zone. A similar correlation between the development of back arc thrusting and structure in the back arc has been suggested by Silver [1979] for the distribution of back arc thrusting behind the southern Banda arc where collision with the Australian continent is now taking place.

I interpret the zone of earthquakes in the eastern Gorontalo Basin (Figure 3) as occurring mainly at the southern end of a small tab of lithosphere possibly attached to the slab subducted beneath the Celebes Sea. The bend in the contours near the North Arm of Sulawesi (Figure 10), modified from those of Cardwell et al. [1980], indicates that the tab beneath the Gorontalo Basin is bent up relative to the remainder of the slab to the north. The bending of this small tab at the southern extreme of the subducted plate is interpreted as an effect of the counterflow of asthenosphere laterally (southward) away from the arc-arc collision in the central Molucca Sea and may represent streamlining of the slab as it sinks into the mantle.

Appendix

In November and December of 1978, portable seismograph stations were operated on the islands of Mayu, Tifore, Ternate, and Sangihe, and a fifth station alternated between Banggai and Luwuk (Figure 1) for 21 days. Permanent stations at Manado, Makassar, Ambon, Balikpapan and Mindanao [Hodgson, 1980] were also used as sources of arrival time data (see Figure 1). Local arrival time data were supplemented by the Earthquake Data Report of the U.S. Geological Survey and phase report sheets from other regional stations in Indonesia and the Philippines.

Portable instruments used were two Sprengnether MEQ-800's and three Kinemetrics PS-1A's. Short-period vertical seismometers were used at all stations. Arrival times of phases were picked with an accuracy of 0.2 s for impulsive P and 0.5 s for emergent P phases on the Sprengnether records, which were operated at 120 mm/min (smoked paper). The Kinemetrics instruments were run at a drum speed of 60 mm/min and used an ink trace, so accuracy of picking phases is slightly less than that for the Sprengnether records (0.3 and 1. s for impulsive and emergent P phases, respectively). S phases are picked within 1. s for all arrivals.

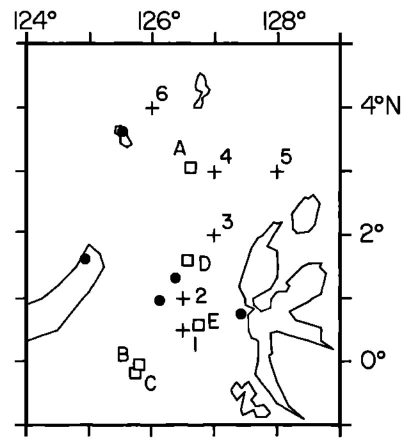

Fig. A1. Locations of test events (pluses) shown in Figure A2 and earthquakes (squares) shown in Figure A3 used in error analyses discussed in the appendix.

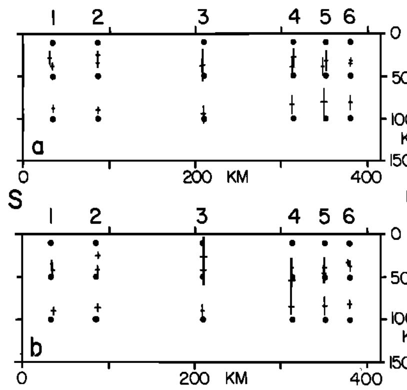

Fig. A2. Vertical section of test events shown in Figure A1. The projection angle is N20°E. Circles show actual locations of each event, and pluses show means and errors of one standard deviation in relocating the event 20 times while adding random errors to the arrival times. (a) Results without the use of station delays. (b) Results using station delays computed by the JHD method. Each event is numbered as in Figure A1 and Table A2. Velocity models used to generate and locate events are given in Table A1.

Hypocenters were located using the methods of joint hypocenter determination [Dewey, 1971] and single-event location [Bolt, 1960]. The most extensively recorded events were located and station delays were calculated by JHD. All events were located with the single-event program utilizing calculated residuals at stations and variances for phases. This strategy in locating earthquakes is preferable to locating all events by the JHD in separate groups (the JHD can locate only 15 events per run), in which case, groups may shift relative to each other owing to the use of different station residuals calculated from each group [Dewey, 1971]. Travel time tables for

Table A1. Velocity Models

V_P, km/s	V_S, km/s	Depth, km
	Test Model	
5.0	2.8	0.
6.5	3.6	5.
7.3	4.0	11.
8.0	4.7	20.
	Model Used at Mayu and Tifore	
2.7	1.5	0.
4.1	2.3	5.
6.2	3.4	14.
8.0	4.5	21.

Table A2. Computed Hypocenters for Test Earthquakes

	True Position			Latitude, °N		Longitude, °E		Depth, km		Origin Time	
Site	Latitude, °N	Longitude, °E	Depth, km	Mean	SD	Mean	SD	Mean	SD	Mean	SD
			Locations With No Delays Used								
1	0.5	126.5	10	0.48	0.02	126.46	0.00	27.9	7.9	2.18	0.49
			50	0.50	0.02	126.48	0.00	38.0	3.9	1.09	0.42
			100	0.51	0.02	126.48	0.00	87.9	4.2	2.18	0.37
2	1.0	126.5	10	1.01	0.02	126.46	0.04	24.8	5.0	2.24	0.56
			50	1.01	0.02	126.47	0.00	34.0	5.2	1.35	0.41
			100	1.00	0.02	126.50	0.05	90.0	3.9	2.10	0.42
3	2.0	127.0	10	2.00	0.02	126.95	0.00	37.3	18.3	3.01	0.84
			50	1.99	0.02	126.96	0.00	37.6	7.6	1.29	0.51
			100	1.99	0.02	127.00	0.02	94.9	9.9	2.11	0.37
4	3.0	127.0	10	3.00	0.02	127.00	0.04	27.7	10.2	2.29	0.80
			50	2.99	0.02	126.98	0.05	39.7	11.1	4.21	1.52
			100	2.98	0.02	127.01	0.01	83.7	10.6	1.76	0.64
5	3.0	128.0	10	3.01	0.02	127.97	0.00	32.1	11.9	2.48	0.91
			50	2.98	0.02	127.94	0.00	39.1	10.4	1.54	0.63
			100	2.99	0.03	127.96	0.06	81.0	15.7	2.11	0.63
6	4.0	126.0	10	4.00	0.01	125.99	0.04	31.8	3.1	2.54	0.33
			50	3.99	0.02	126.01	0.04	35.5	3.8	1.24	0.36
			100	3.98	0.02	126.04	0.00	81.6	8.5	2.03	0.28
			Locations With JHD Delays Included								
1	0.5	126.5	10	0.50	0.03	126.52	0.00	34.8	4.7	6.69	0.48
			50	0.51	0.02	126.51	0.00	41.7	8.2	4.75	0.38
			100	0.52	0.02	126.53	0.05	90.2	5.0	5.98	0.46
2	1.0	126.5	10	1.02	0.02	126.49	0.06	25.0	3.7	6.17	0.36
			50	1.01	0.02	126.50	0.05	41.7	4.1	4.79	0.29
			100	1.01	0.02	126.52	0.05	86.5	4.5	6.31	0.48
3	2.0	127.0	10	2.01	0.03	126.99	0.06	26.5	23.4	5.93	2.27
			50	2.02	0.03	126.96	0.07	41.8	17.3	5.20	1.62
			100	1.99	0.02	127.01	0.00	89.5	7.5	6.08	0.46
4	3.0	127.0	10	2.99	0.01	126.99	0.05	38.9	9.1	7.34	0.77
			50	3.00	0.03	126.97	0.06	53.9	25.8	5.45	1.47
			100	2.99	0.02	127.00	0.04	84.9	8.9	6.28	0.44
5	3.0	128.0	10	3.00	0.02	127.97	0.06	38.6	11.9	7.19	1.03
			50	3.00	0.02	127.96	0.00	46.0	10.3	5.33	0.94
			100	3.00	0.02	127.98	0.04	83.9	10.5	6.23	0.57
6	4.0	126.0	10	3.99	0.02	125.97	0.07	32.8	4.0	7.15	0.62
			50	4.00	0.01	126.00	0.04	36.9	6.5	4.66	0.58
			100	3.99	0.02	126.02	0.07	81.7	4.7	6.33	0.33

P and pP were taken from Herrin et al. [1968] and for S from Jeffreys and Bullen [1958] except at the Mayu and Tifore stations, where a local travel time curve was incorporated to represent velocity structure as determined from refraction profiles near these islands [McCaffrey et al., 1980a] (Table A1).

In order to estimate accuracy in locating the recorded earthquakes with the given array geometry, several tests were conducted. Test hypocenters were generated at 10-, 50-, and 100-km depths at six sites (Figure A1) and arrival times at stations were calculated, assuming arbitrary travel time curves for P and S (Table A1). The origin time of each event is 0001:00. In order to estimate the upper limit on expected accuracy of hypocenter determinations, these test events were located by the single-event location scheme while using the travel time tables from which they were generated. To test the effect of varying trial hypocenters and origin times, initial hypocentral parameters were randomly perturbed from their true positions by several degrees and from their true origin times by several seconds. This test represents ideal conditions of known velocity structure and perfect arrival time data, thus any errors encountered in finding the true source parameters are due to either poor convergence of the location scheme (i.e., dependence on the trial hypocenter) or nonideal network geometry with respect to the hypocenter. The results of this test indicate that the final solution does not display significant dependence on the starting values of the hypocenter.

The test described above represents the ideal case for the local network. In reality, the velocity structure is not exactly known, errors are present in reading arrival times of phases, and both phases (P and S) are not recorded by all stations for all events. Each of these conditions introduces an additional degree of uncertainty to the calculated hypocentral parameters and are examined in turn.

The effects of errors in reading arrival times were examined by relocating both the observed earthquakes and the synthetic events while adding random errors to arrival times. Random errors with a mean of zero and standard deviation of 1.0 s were added to the arrival times of both P and S phases during 20 runs of the single-event location program. During these runs the Herrin

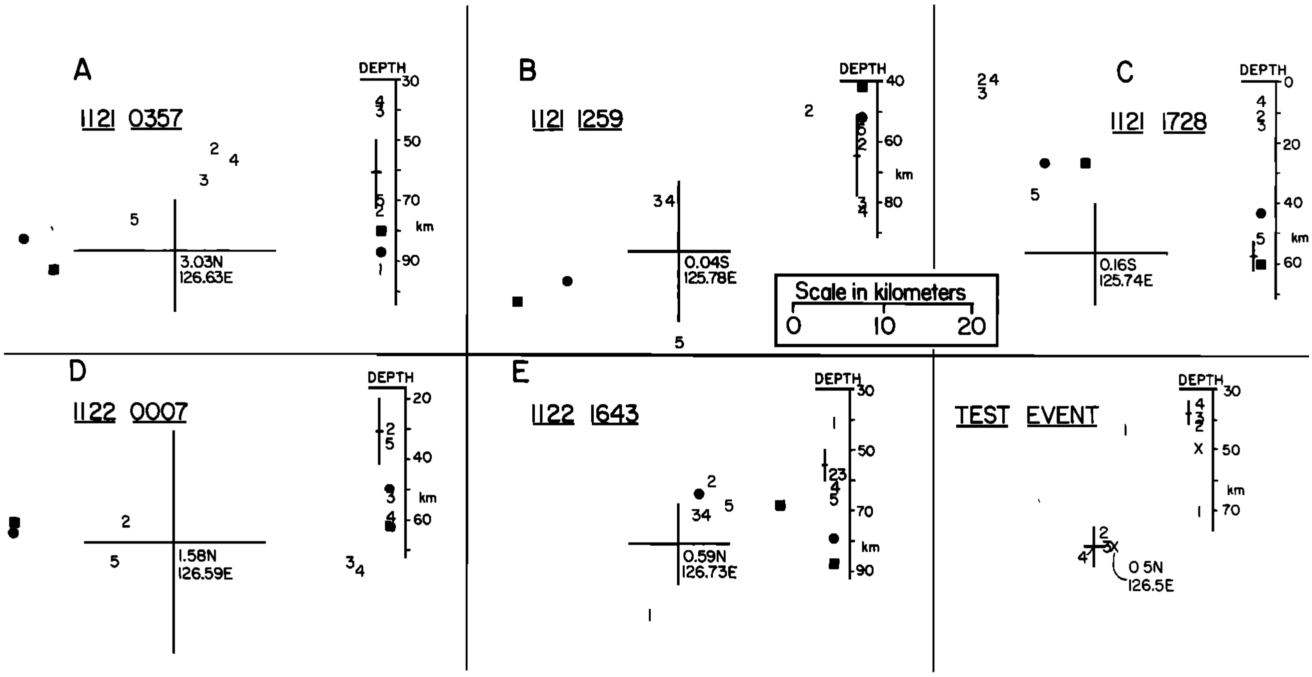

Fig. A3. Results of relocating five earthquakes and one test event while using subsets of the recording stations. Locations of events are shown in Figure A1. Error bars of one standard deviation are given for each event, and the mean epicenter is shown in the southeast quadrant. The subsets are coded (by numbers) as follows: (1) data only from Mayu, Tifore, Ternate, and station MNI, (2) Luwuk and Sangihe added, (3) stations AAI, MKS, and DAV added, (4) stations CGP, MPP, KKM, BPK, and KUPT added, and (5) all available data used. On the right-hand side the corresponding depth determinations are shown for each subset. The solid circles are EDR locations, and the solid squares are from the ISC. For the test event the cross marks the true position.

tables and local crustal model were employed. The resulting shifts in epicenters and depths for the test events are shown in Figure A2 and are tabulated in Table A2. The center of each plus in Figure A2 is on the mean of the 20 locations, and the lengths of the arms represent one standard deviation from the mean in each direction. Figure A2a displays the results of locating the test events without station delays, and Figure A2b shows the results using station delays computed in a JHD solution for the test events. Figure A2 suggests that the locations determined by the two methods are not significantly different, and Table A2 shows that the effect of using station delays (which ranged from -3.0 to -5.0 s) was to change the origin time rather than to improve the depth calculation. This feature indicates a strong origin time-depth coupling problem in the least squares solutions for these earthquakes.

In the four-parameter least squares approach to the hypocenter location problem (as has been used here), the largest instability is due to nonindependent behavior between the four variables: origin time, latitude, longitude, and depth. This instability, which is dependent on network configuration with respect to the hypocenter, is best exposed by relocating earthquakes using subsets of the recording stations. Several of the observed events from the Molucca Sea displayed large average shifts in hypocentral parameters (tens of kilometers in epicenter and depth) while using some subsets of the stations (Figure A3). Shifts in computed locations of test events under similar perturbations were generally much smaller than those of the observed data (Figure A3). Relocating the test events with varying numbers of stations and phases (P and S) suggests that at least five P and two S phases are needed to locate events well throughout most of the region, and this criterion was applied to all earthquakes presented in this paper. The dependence of location on the number and spatial distribution of stations suggests either substantial instability in the least squares solution or strong lateral variations in velocity.

The stations at Mayu and Tifore, on the Talaud-Mayu Ridge, overlie a thick, low-velocity crustal layer, and a corrective crustal model based on refraction profiles [McCaffrey et al., 1980a] was used in calculating travel times to these stations (Table A1). Mantle velocities for both P (8.0 km/s) and S (4.5 km/s) were determined from arrival time data from shallow earthquakes. Figure A4a shows a plot of P and S wave travel times as a function of distance out to 300 km. Superimposed on the plot are the local P and S, the Herrin et al. [1968] P, and the Jeffreys and Bullen [1958] S travel time curves. The S wave arrival time data suggest a slightly lower velocity than that used in the velocity models, but the scatter prevents a well-constrained velocity determination. Figure A4b is a plot of the ratio of S wave to P wave travel time (equivalent to V_p/V_s) plotted as a

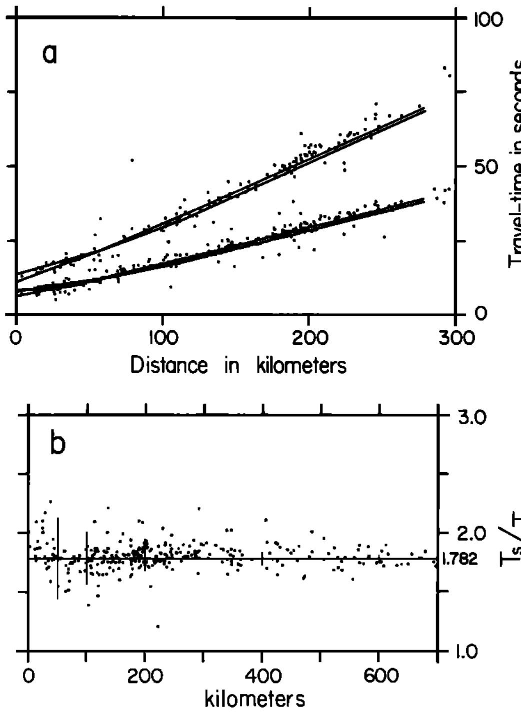

Fig. A4. (a) Travel times of P and S for shallow (h < 50 km) earthquakes in the Molucca Sea. The solid lines show the travel time curves used in the location procedure and are (from top to bottom) local S curve, Jeffreys-Bullen S, local P, and Herrin P. (b) Plot of ratio of S wave travel time to P wave travel time for earthquakes in the Molucca Sea. The horizontal line is the mean of all observations, and the vertical bars represent the range of values (at the given distance) expected if there were a random error of 1.0 s in both P and S travel times. Systematic errors (such as in the origin time) lead to much smaller variation in the ratio of T_s/T_p.

function of distance. The mean value for V_p/V_s from these observations is 1.782 ± 0.158, a value close to that determined for Japan and oceanic regions but higher than that for continental areas [Hales and Muirhead, 1980].

The result of assuming a realistic crustal model beneath Mayu and Tifore was to reduce near-station residuals to acceptable values relative to the global averages for the larger events with little effect on depth and origin times. For smaller events, which fewer stations recorded, calculated depths of events became shallower by 5-15 km after the inclusion of the local travel time curves.

Acknowledgments. Many people contributed to the field work and analyses presented in this paper. E. A. Silver was invaluable in offering logistical and scientific advice. The Indonesian Government and, in particular, the Geological Research and Development Centre, Ministry of Mines, and the Institute of Meteorology and Geophysics were very cooperative. H. M. S. Hartono, J. Widartoyo, R. Susanto, and Y. S. Joyodiwiryo are gratefully acknowledged for their help in arranging the field work. R. Buyung, R. Sutardjo, Sukarman B., M. Husni, Suciono, D. Satuju, and E. Sukamto operated portable stations for portions of the survey period. P. Molnar and S. Roecker lent us instruments. R. Lenz spent many hours at the terminal punching in data. T. J. Fitch and J. W. Dewey offered advice, information, and computer programs. I thank E. A. Silver, P. Molnar, and one anonymous reviewer for many helpful suggestions. Last, but not least, I thank the many wonderful people of eastern Indonesia who have made field work in that part of the world a pleasure. The field work was supported by grants from the H. O. Wood Foundation of the Carnegie Institution of Washington, the Geological Society of America, and Sigma Xi, the Scientific Research Society of North America. The author was supported by NSF grants OCE76-020365, EAR77-10034, and OCE78-08693 during the period in which this work was conducted.

References

Bath, M., and S. J. Duda, Some aspects of global seismicity, Tectonophysics, 54, T1-T8, 1979.

Bird, P., M. N. Toksoz, and N. H. Sleep, Thermal and mechanical models of continent-continent convergence zones, J. Geophys. Res., 80, 4405-4416, 1975.

Bolt, B. A., The revision of earthquake epicenters, focal depths, and origin times using a high-speed computer, Geophys. J. R. Astron. Soc., 3, 433-440, 1960.

Cardwell, R. K., B. L. Isacks, and D. E. Karig, The spatial distribution of earthquakes, focal mechanism solutions and plate boundaries in the Philippine and northeastern Indonesian islands, in The Tectonic and Geologic Evolution of Southeast Asian Seas and Islands, Geophys. Monogr., vol. 23, edited by D. E. Hayes, pp. 1-35, AGU, Washington, D. C., 1980.

Dewey, J. W., Seismicity studies with the method of joint hypocenter determination, Ph.D. thesis, Univ. of Calif., Berkeley, 1971.

Duda, S. J., Secular seismic energy release in the circum-Pacific belt, Tectonophysics, 2, 409-452, 1965.

Engdahl, E. R., Seismicity and plate subduction in the central Aleutians, in Island Arcs, Deep Sea Trenches and Back-Arc Basins, Maurice Ewing Ser., vol. 1, edited by M. Talwani and W. C. Pitman III, pp. 259-272, AGU, Washington, D. C., 1977.

Fitch, T. J., Earthquake mechanisms and island arc tectonics in the Indonesian-Philippine region, Bull. Seismol. Soc. Am., 60, 565-591, 1970.

Fitch, T. J., Plate convergence, transcurrent faults, and internal deformation adjacent to southeast Asia and the western Pacific, J. Geophys. Res., 77, 4432-4460, 1972.

Fitch, T. J., and P. Molnar, Focal mechanisms along inclined earthquake zones in the Indonesian-Philippine region, J. Geophys. Res., 75, 1431-1444, 1970.

Hales, A. L., and K. J. Muirhead, The ratio of the travel times for S and P at distances less than 10°, Bull. Seismol. Soc. Am., 70, 823-829, 1980.

Hamilton, W., Earthquake map of the Indonesian

region, scale 1:5,000,000, U.S. Geol. Surv., Misc. Invest. Ser., Map I-875-C, 1974.
Hamilton, W., Subduction in the Indonesian region, in Island Arcs, Deep Sea Trenches and Back-Arc Basins, Maurice Ewing Ser., vol. 1, edited by M. Talwani and W. C. Pitman III, pp. 15-31, AGU, Washington, D. C., 1977.
Hamilton, W., Tectonics of the Indonesian region, U.S. Geol. Surv. Prof. Pap., 1078, 345 pp., 1979.
Hatherton, T., and W. R. Dickinson, The relationship between andesitic volcanism and seismicity in Indonesia, the Lesser Antilles, and other island arcs, J. Geophys. Res., 74, 5301-5310, 1969.
Herrin, E., et al., 1968 seismological tables for P-phases, Bull. Seismol. Soc. Am., 58, 1193-1352, 1968.
Hodgson, J. H., A short-period seismograph network in Southeast Asia, Bull. Seismol. Soc. Am., 70, 385-392, 1980.
International Seismological Centre, Bulletin of the International Seismological Centre, Newbury, United Kingdom, 1964-1975.
Jackson, J., Errors in focal depth determination and the depth of seismicity in Iran and Turkey, Geophys. J. R. Astron. Soc., 61, 285-301, 1980.
Jackson, J., and T. J. Fitch, Seismotectonic implications of relocated aftershock sequences in Iran and Turkey, Geophys. J. R. Astron. Soc., 57, 209-229, 1979.
Jackson, J., and T. J. Fitch, Basement faulting and the focal depths of the larger earthquakes in the Zagros Mountains (Iran), Geophys. J. R. Astron. Soc., 64, 561-586, 1981.
Jeffreys, H., and E. Bullen, Seismological tables, 50 pp., Br. Assoc., Gray-Milne Trust, London, 1958.
Karig, D. E., Basin genesis in the Philippine Sea, in Initial Reports of the Deep Sea Drilling Project, vol. 31, pp. 857-879, U.S. Government Printing Office, Washington, D. C., 1975.
Kelleher, J., and W. McCann, Buoyant zones, great earthquakes, and unstable boundaries of subduction, J. Geophys. Res., 81, 4885-4896, 1976.
Mammerickx, J., R. L. Fisher, F. J. Emmel, and S. M. Smith, Bathymetry of the east and southeast Asian seas, Map Chart Ser., MC-17, Geological Society of America, Boulder, Co., 1976.
McCaffrey, R., E. A. Silver, and R. W. Raitt, Crustal structure of the Molucca Sea collision zone, Indonesia, in The Tectonic and Geologic Evolution of Southeast Asian Seas and Islands, Geophys. Monogr., vol. 23, edited by D. E. Hayes, pp. 161-178, AGU, Washington, D. C., 1980a.
McCaffrey, R., R. Sutardjo, and R. Susanto, Local earthquake survey of the Molucca Sea collision zone, Indonesia (abstract), Eos Trans. AGU, 61, 1045, 1980b.
McCaffrey, R., E. A. Silver, and R. W. Raitt, Seismic refraction studies in the East Arm, Sulawesi-Banggai Islands region of eastern Indonesia, in The Geology and Tectonics of Eastern Indonesia, edited by H. M. S. Hartono and A. J. Barber, Geological Research and Development Centre, Bandung, Indonesia, in press, 1981.
Morrice, M. G., and J. B. Gill, Regional geochemistry of the Sangihe volcanic arc, Indonesia (abstract), Eos Trans. AGU, 61, 1140, 1980.
Niazi, M., I. Asudeh, G. Ballard, J. Jackson, G. King, and D. McKenzie, The depth of seismicity in the Kermanshah region of the Zagros Mountains (Iran), Earth Planet. Sci. Lett., 40, 270-274, 1978.
Pascal, G., B. L. Isacks, M. Barazangi, and J. Dubois, Precise relocations of earthquakes and seismotectonics of the New Hebrides island arc, J. Geophys. Res., 83, 4957-4974, 1978.
Savage, W. U., J. N. Alt, and A. Mohajer-Ashari, Microearthquake investigations of the 1972 Qir, Iran, earthquake zone and adjacent areas, Geol. Soc. Am. Program Abstracts, 496, 1977.
Seno, T., The instantaneous rotation vector of the Philippine Sea plate relative to the Eurasian plate, Tectonophysics, 42, 209-226, 1977.
Silver, E. A., Back-arc thrusting (abstract), Eos, Trans. AGU, 60, 958, 1979.
Silver, E. A., A new tectonic map of the Molucca Sea and East Sulawesi, Indonesia, with implications for hydrocarbon potential and metallogenesis, in, The Geology and Tectonics of Eastern Indonesia, edited by H. M. S. Hartono and A. J. Barber, Geological Research and Development Centre, Bandung, Indonesia, in press, 1981.
Silver, E. A., and J. C. Moore, The Molucca Sea collision zone, Indonesia, J. Geophys. Res., 83, 1681-1691, 1978.
Stewart, G. S., and S. N. Cohn, The 1976 August 16, Mindanao, Philippine earthquake (Ms=7.8) --- Evidence for a subduction zone south of Mindanao, Geophys. J. R. Astron. Soc., 57, 51-65, 1979.
Sykes, L. R., B. L. Isacks, and J. Oliver, Spatial distribution of deep and shallow earthquakes of small magnitudes in the Tonga-Fiji region, Bull. Seismol. Soc. Am., 59, 1093-1113, 1969.
U.S. Geological Survey, Earthquake Data Report, Arlington, Va, Nov.-Dec., 1978.
Von Dollen, F. J., J. N. Alt, D. Tocher, and A. Nowroozi, Seismologic and geologic investigations near Bandar Abbas, Iran, Geol. Soc. Am. Program Abstracts, 521, 1977.
Watts, A. B., J. H. Bodine, and C. O. Bowin, Free-air gravity field, in A Geophysical Atlas of East and Southeast Asian Seas, edited by D. E. Hayes, Map Chart Ser. MC-25, Geological Society of America, Boulder, Co., 1978.

(Received March 30, 1981;
revised July 30, 1981;
accepted September 11, 1981.)